Generation of tunable blue–green light using ZnO periodically poled lithium niobate crystal fiber by self-cascaded second-order nonlinearity

Li-Min Lee,[1,2] Shan-Chuang Pei,[3,4] Der-Fong Lin,[5] Po-Chun Chiu,[5] Mon-Chang Tsai,[1] Ta-Min Tai,[1] De-Hao Sun,[3] A. H. Kung,[4,6] and Sheng-Lung Huang[7,*]

[1]*Institute of Electro-Optical Engineering, National Sun Yat-Sen University, Kaohsiung 804, Taiwan*
[2]*Department of Electrical Engineering, Yung Ta Institute of Technology & Commerce, Pingtung 909, Taiwan*
[3]*Graduate Institute of Electro-Optical Engineering, National Taiwan University, Taipei 106, Taiwan*
[4]*Institute of Atomic and Molecular Sciences, Academia Sinica, Taipei 106, Taiwan*
[5]*Institute of Communications Engineering, National Sun Yat-Sen University, Kaohsiung 804, Taiwan*
[6]*Department of Photonics, National Chiao Tung University, Hsinchu 300, Taiwan*
[7]*Department of Electrical Engineering and Graduate Institute of Electro-Optical Engineering, National Taiwan University, Taipei 106, Taiwan*
[*]*Corresponding author: slhuang@cc.ee.ntu.edu.tw*

Received January 8, 2007; revised April 13, 2007; accepted April 15, 2007;
posted April 24, 2007 (Doc. ID 78763); published July 19, 2007

Using a novel self-cascaded first-order second-harmonic generation (SHG) and third-order sum-frequency generation (SFG) in a ZnO periodically poled lithium niobate crystal fiber, tunable blue–green light was demonstrated. At a domain pitch of 15.45 μm, the SHG signal and its fundamental signal at 1423.9 nm can satisfy the third-order SFG quasi-phase-matched (QPM) condition. The measured SHG power at 714.2 nm was 12.25 mW under 100 mW input power, and the estimated nonlinear coefficient (d_{33}) achieved was 25.3 pm/V. The self-cascaded SHG+SFG power measured at 477.1 nm was ~700 μW under 350 mW input power. The maximum internal efficiency of the SHG is 14.84%. The tuning range of the self-cascaded SHG and SFG generated tunable blue–green light was more than 40 nm, from 471.3 to 515 nm. The maximum simulated 3 dB bandwidth achieved using a gradient-period QPM structure is 196 nm, which is from 1476 to 1672 nm. The gain-bandwidth product of the self-cascaded SHG and SFG processes decreases drastically as the bandwidth is broadened. © 2007 Optical Society of America

OCIS codes: 190.4400, 160.3730, 140.3600.

1. INTRODUCTION

Blue–green light sources are desired for many applications, such as projection television, satellite communication, underwater communication, and biomedical analysis. Many approaches have been attempted for the generation of tunable blue–green coherent light sources. Intracavity second-harmonic generation (SHG) [1–3] using a fan structure was demonstrated with a tuning range of 10 nm (480.4–490.6 nm) [4]. The optical parametric process has been an effective means for tunable laser generation [5,6], but there were few demonstrations that generated blue–green light [7,8]. More than 20 nm of tunable blue light (425–445 nm) was demonstrated using optical parametric generation and sum-frequency generation (SFG) [9]. Tunable femtosecond laser pulses (380–460 nm) were generated from a 405 nm pumped type I β-BaB_2O_4 (β-BBO) noncollinear optical parametric amplifier where two β-BBO crystals were used for SHG and SFG [10]. Quasi-phase-matched (QPM) nonlinear conversion [11] enables the use of the largest nonlinear coefficient of a particular nonlinear crystal. Periodically poled lithium niobate (PPLN) is a well-known nonlinear crystal [12]. Its frequency conversion bandwidth can be engineered with variation of the domain pitch [13]. To reduce the photorefractive damage [14], Mg or Zn ions are used. It has also been pulled into crystal fiber so that the required material consumption can be reduced [15]. A PPLN crystal fiber sample with a domain pitch of 15.45 μm was fabricated by an *in situ* electric-field-induced microswing poling technique during crystal fiber growth by the laser-heated pedestal growth (LHPG) method [16]. The cascaded SHG and SFG scheme has the advantage of easy coupling [17]. In this paper, what we believe to be a novel and simple self-cascaded SHG+SFG scheme is presented for the generation of tunable blue–green light using ZnO-doped PPLN crystal fiber (PPLNCF) with a single designed pitch. With gradient-domain period in the QPM structure, the self-cascaded SHG+SFG bandwidth can be broadened.

To characterize the PPLNCF, a 4 kHz repetition rate PPLN-based optical parametric oscillator (OPO) pulsed laser with a pulse duration of 27 ns was employed. The measured SHG power at 714.2 nm was 12.25 mW under 100 mW input power, and the nonlinear coefficient (d_{33}) estimated was 25.3 pm/V. The self-cascaded SHG+SFG power measured at 477.1 nm was 700 μW under 350 mW input power with a tuning range from 471.3 to 515 nm. To broaden the bandwidth of the cascaded χ^2 process and improve the conversion efficiency, a gradient-period QPM structure is considered. The design criteria are presented

 © 2007 Optical Society of America

and discussed. The maximum 3 dB bandwidth by simulation is 161 nm, from 1476 to 1637 nm. The gain-bandwidth products of SHG or SFG do not decrease as the bandwidths are extended, but the gain-bandwidth product of the self-cascaded SHG+SFG decreases appreciably as the bandwidth is broadened.

2. DEVICE CONCEPT AND FABRICATION

The concept of the self-cascaded SHG+SFG is depicted in Fig. 1(a), where the addends for the SFG are the fundamental wavelength and its SHG. The phase-matching temperature is 25°C. The required QPM pitch for the first-order SHG is the same as that of the third-order SFG at a wavelength of 1423.9 nm, which means both χ^2 processes can satisfy QPM simultaneously. The corresponding domain pitch is 15.45 μm. This cascaded process is similar to $\chi 3$ process, so the third harmonics can be generated using this scheme. The simulated SHG and self-cascaded SHG+SFG efficiencies are shown in Fig. 1(b). Also shown in Fig. 1(a) is that the dependence of the two χ^2 processes on wavelength are quite parallel around the wavelength of 1423.9 nm, which suggests the possibility of broadband tuning.

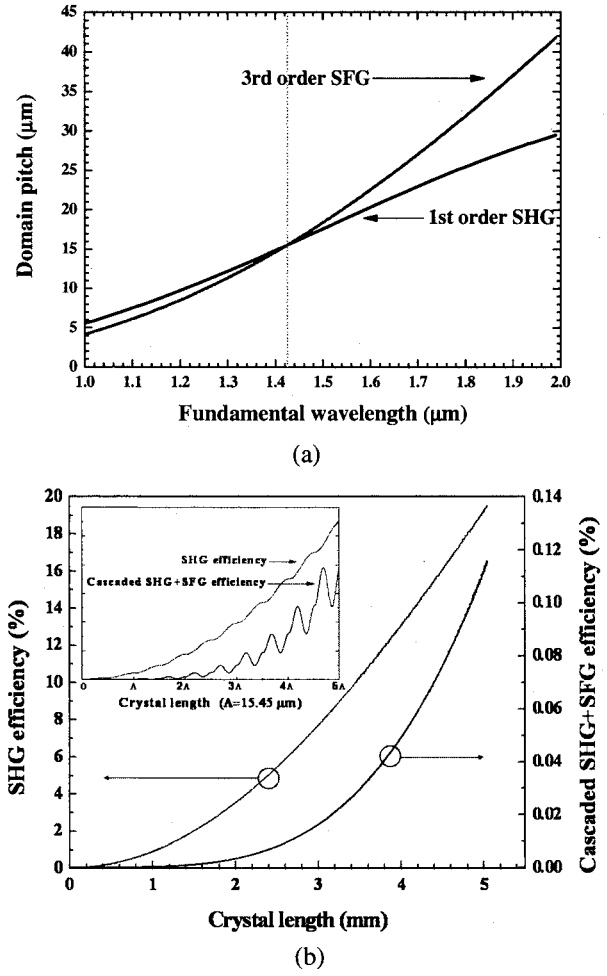

Fig. 1. (a) QPM conditions for the first-order SHG and the third-order SFG (fundamental wavelength and its SHG) in the near-infrared range. (b) Simulated SHG and self-cascaded SHG +SFG efficiencies. The inset is an expanded view.

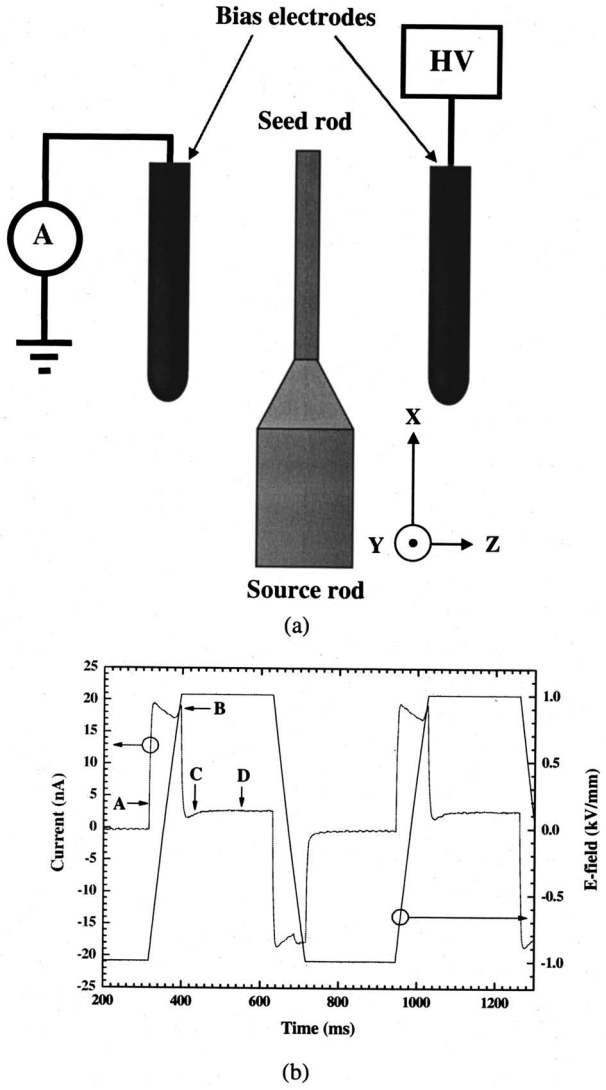

Fig. 2. (a) Displacement current measurement setup. (b) Measured current and the applied voltage waveforms. The markers A, B, C, and D correspond to the current responses due to the applied voltage positive slope, the applied voltage positive slope added the induced charges increasing rate, the induced charges increasing rate, and the constant increasing rate of induced charges, respectively.

The PPLNCF was fabricated by an *in situ* electric-field-induced microswing poling technique during crystal fiber growth by the LHPG method. The lithium niobate (LN) source rod was X cut with a 6 mol. % ZnO doping and a cross section of 500 μm $\times$ 500 μm. The seed rod grown from the source rod was also X cut. The crystal orientation of the setup is shown in Fig. 2(a). A pair of electrodes separated by 3 mm was used to pole the just-grown crystal fiber. The 6 mol. % ZnO-doped LN has similar damage threshold and photorefractive resistance compared to that of a 5 mol. % MgO-doped LN [18], but after poling, ZnO-doped PPLNCF usually has better domain pattern in term of uniformity. The growth speed was 1.8 mm/min with a pull–push speed ratio of 9/1.

To pole through the crystal fiber cross section, the free-charge screening effect near the molten zone should be reduced so that the applied electric field can penetrate the

fiber. The slight swing of the just-grown fiber tip due to the applied electric field was carefully controlled to have stable growth and poling. The swing amplitude, usually a few tens of micrometers, is influenced by many factors, such as the electrostatic force resulted from the induced mirror charges by the applied electric field and pyroelectric charges in the high-temperature region, the stiffness of grown crystal fiber, and the surface tension of the melt. The stiffness depends on the length of grown crystal fiber, the fiber diameter, and the stiffness of seed rod mounting. All the growth conditions are elaborately kept the same to have uniform fiber diameter and poled pattern. With real-time image monitoring, the microswing amplitude was precisely maintained using the displacement current from the applied electric field as the feedback signal. The melt shape was maintained with stable CO_2 power. If the variation of melt shape or swing amplitude is out of a tolerance, the uniformity of the poled pattern will lose. The tolerance will be discussed later. The displacement current was monitored by a picoammeter during the PPLNCF growth. The measured current and the applied voltage waveform are illustrated in Fig. 2(b). The measured displacement current, $i(t)$, and the induced charges, Q_i, in the just-grown fiber tip can be expressed as

$$i(t) = C_e \frac{dV_a(t)}{dt} + \frac{dQ_i(t)}{dt},$$

$$Q_i(t) = k_1 \frac{V_a^2(t)}{[l_o/2 - D(t)]^2} + k_2 t (V_s - V_t)^2, \quad (1)$$

where C_e is the equivalent capacitor between the electrodes, V_a is the periodically applied voltage, l_o is the separation between the electrodes, $D(t)$ is the deflection length of the just-grown fiber tip from the growth axis, V_s is the peak applied voltage, V_t is the threshold voltage, and k_1, k_2 are constants. The current is composed of effective capacitive current and induced-charge current. Section A in Fig. 2(b) is attributed to the first term in the current equation, which arises from the positive rising slope of the applied voltage. The current drops gradually due to the capacitor discharges. Section B in Fig. 2(b) resulted from the increasing of the induced charge, when the grown fiber tip moves closer toward the right electrode. The closer the grown fiber moves toward the right electrode, the more the induced charges are generated. When the applied voltage becomes constant, the first term in current equation becomes zero and the peak current drops, but the second term in current equation increases continuously through section C to section D as Fig. 2(b) shows. The first term in the charge equation corresponds to a state while the fiber tip moves toward the electrodes. The quadratic relation is attributed to the product of electric field and the effective area of the induced charges. The constant current level in section D is coined "stair current." It is kept constant because the increasing rate of the induced charges is constant, as the fiber tip pauses at the right- and left-most positions. The stair-current level depends on the square of the static applied voltage and has a threshold. The second term of the charge equation models the constant increasing rate of the induced charges when the applied voltage is static. In addition, near the molten zone where the temperature is high, the dependence of the required poling field to invert the dipoles becomes nonlinear. To account for this effect, a quadratic relation between Q_i and V_s is used. Below a threshold voltage, V_t, the induced charges are negligible because of the relative charge stabilization energy. A CCD camera was used to record the microswing images and $D(t)$. The

Table 1. Parameters Used to Simulate the Displacement Current

Parameters	Value	Unit
Applied voltage		
Peak voltage	3	kV
Repetition rate	1.587	Hz
Rise time	40	ms
Fall time	40	ms
Deflection of the just-grown fiber tip from the growth axis, $D(t)$	70	μm
Equivalent capacitor between the electrodes, C_e	2.7×10^{-13}	F
Constants in the charge equation		
k_1	1×10^{-23}	Coulomb m^2/V^2
k_2	3×10^{-16}	Coulomb/(s V^2)

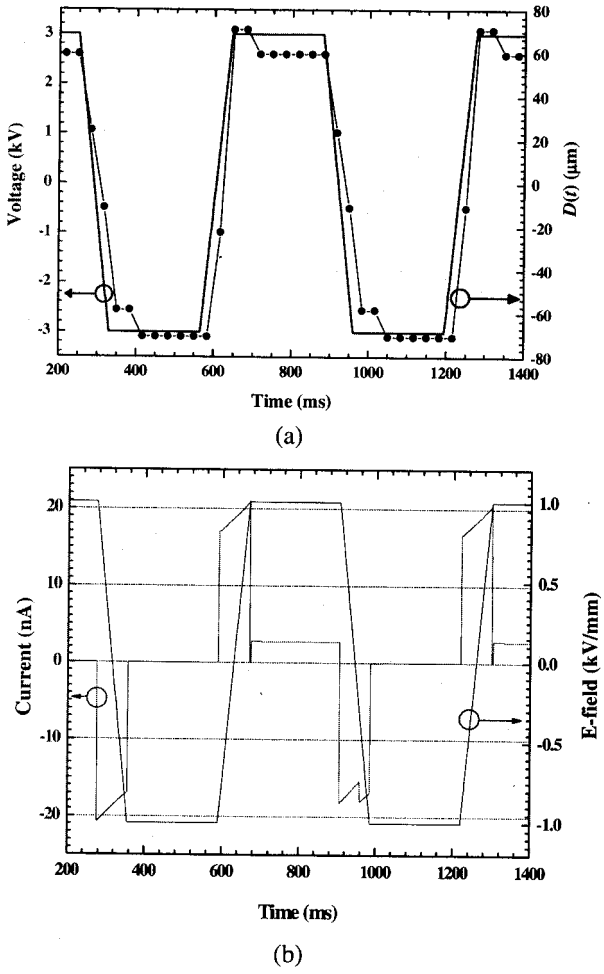

Fig. 3. (a) Applied bias and the measured $D(t)$. (b) Simulated current waveform in relation to the applied E field.

parameters that we used to simulate the displacement current are listed in Table 1. It is observed that the delay of $D(t)$ in response to the applied voltage is ~25 ms as shown in Fig. 3(a). The delay is attributed to the slow response of mechanical inertia. The simulated current waveform as shown in Fig. 3(b) is in good agreement with the measured waveform as shown in Fig. 2(b). The threshold voltage also depends on the swing amplitude. Figure 4(a) shows the dependence of the stair-current level on the applied voltage. The discrepancy between the experiment and simulation is mainly due to the nonlinear effect of applied voltage at temperature near the melting point. The stair current vanishes when the applied voltage is below the threshold voltage, which is ~2.2 kV. The negative stair current is not as pronounced as the positive stair current because the grown crystal fiber tip moves away from the positive electrode due to the negative applied voltage. It should be noted here that the left electrode was grounded. The peak near marker A in Fig. 2(b) depends linearly on swing amplitude as shown in Fig. 4(b). Therefore, the current can be used as an indication for the swing amplitude.

A LABVIEW program was implemented to feedback control the swing amplitude using the current peak. The applied voltage sent to electrodes followed a decreasing function that is optimized by trial and error. The swing amplitude for good poled pattern is within 1.15–1.35 times that of the fiber diameter as shown in Fig. 5(a). As the swing amplitude is below 1.15 times that of the fiber diameter, the crystal fiber cannot be poled through the cross section; while the swing amplitude is over 1.35 times that of fiber diameter, the mechanical vibration of the fiber may stop the stable growth. The CO_2 laser power variation was controlled within 0.3% by the same LABVIEW program with power meter reading to feedback control a rotational polarizer. The result is shown in Fig. 5(a). A PPLNCF with a pitch of 15.45 μm was successfully fabricated. Its cross section after being etched by HF solution is shown in Fig. 5(b). The phase matching conditions for SHG and SFG were calculated from the Sellmeier equation in [19] with slight modification due to the difference in doping concentration.

3. DEVICE CHARACTERIZATION

The test-light source was a grazing-incidence OPO [20] based on QPM PPLN, which was pumped by a commercial laser-diode-pumped acousto-optic Q-switched Nd:YAG laser (Lightwave Electronics Model 610S). The PPLN-OPO pulsed laser has a 4 kHz repetition rate with a continuously tunable wavelength range from 1.4 to 4.5 μm and a pulse duration of 27 ns. The laser output was linearly polarized and the focused beam diameter on the PPLNCF was estimated to be 120 μm. A calibrated prism was used to separate the output light of different wavelengths. Figure 6(a) shows the SHG and self-cascaded SHG+SFG spectra of a sample with a designed domain pitch of 15.45 μm. The SHG conversion efficiency is ~12% at 1428.4 nm, which is 0.4% off the designed wavelength of 1423.9 nm. The length of PPLNCF is 4.5 mm, and the nonlinear coefficient (d_{33}) achieved was 25.3 pm/V, which corresponds to 73% of the value

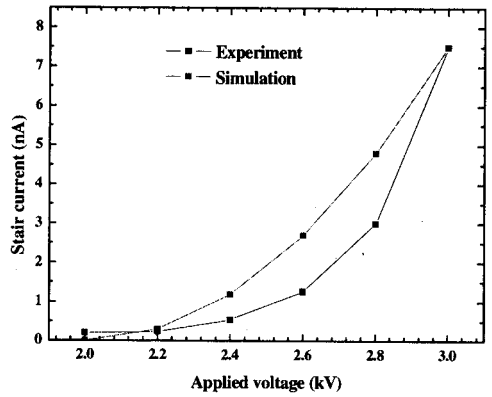

(a)

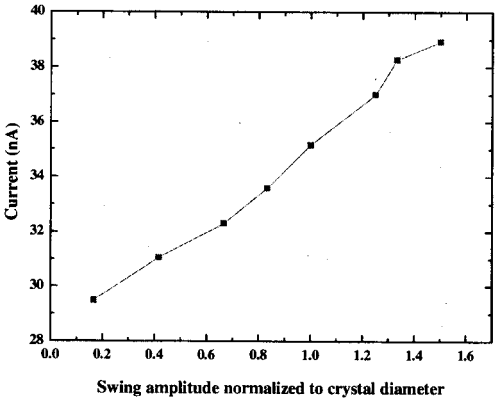

(b)

Fig. 4. (a) Measured and simulated stair currents in response to the applied voltage. (b) Measured peak current is linearly proportional to the normalized microswing amplitude.

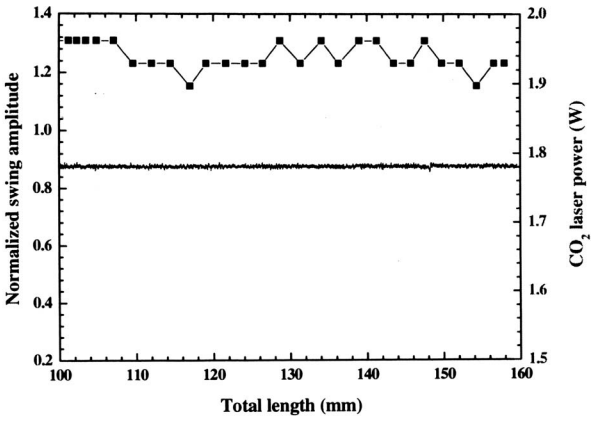

(a)

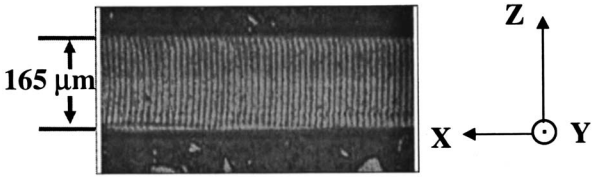

(b)

Fig. 5. (a) Microswing amplitude and CO_2 laser power during the ZnO-doped PPLNCF growth. (b) HF-etched Y-face image of a poled sample with 15.45 μm domain pitch.

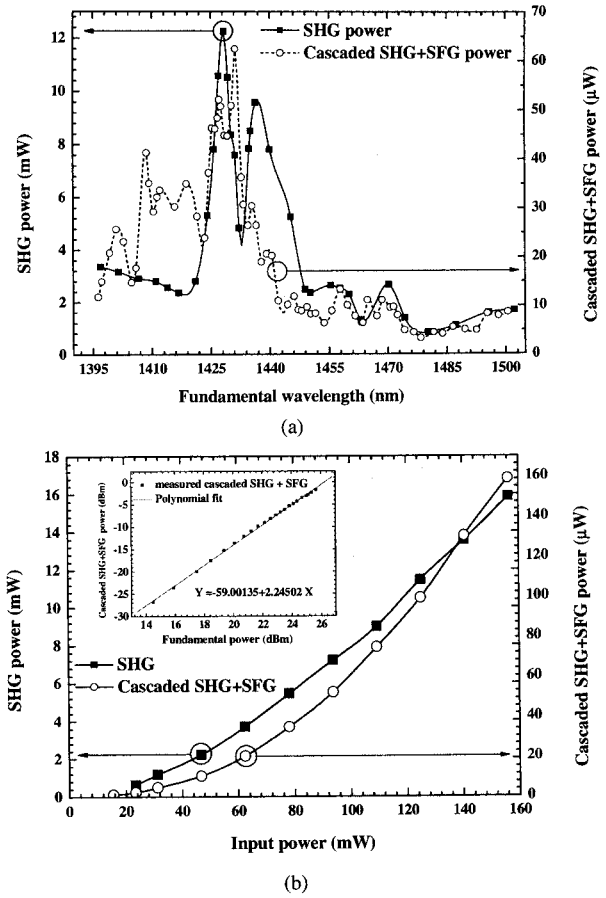

Fig. 6. (a) Generated SHG and self-cascaded SHG+SFG. The peak efficiency of SHG is ~12% at 1428.4 nm and the peak of self-cascaded SHG+SFG is at 477.1 nm. (b) L–I curves of the SHG and self-cascaded SHG+SFG. The inset shows the SHG +SFG power in logarithmic scale.

34.4 pm/V from our source rod vendor, CASIX, Inc. The estimated conversion efficiency is 21.4%. The dip near the center of the SHG spectrum is partly because of the slight variation in domain pitch, and partly due to the energy conversion to the blue–green light. The tuning curve of the self-cascaded SHG+SFG will be further addressed in Section 4. At a fixed-pump wavelength of 1431.3 nm, the conversion efficiencies of the SHG and the cascaded blue–green light were measured as shown in Fig. 6(b). The logarithmic fit of the slope of SHG to the fundamental power is ~1.7, and that of the slope of self-cascaded SHG+SFG is ~2.25 as shown in the inset. The maximum power of blue light was generated at 477.1 nm, which corresponded to fundamental light of 1431.3 nm. The internal blue light achieved was ~700 μW at an OPO power of 350 mW. When the input laser was tuned from 1414 to 1545 nm, the self-cascaded SHG+SFG generated tunable blue–green light from 471.3 to 515 nm as shown in Fig. 7.

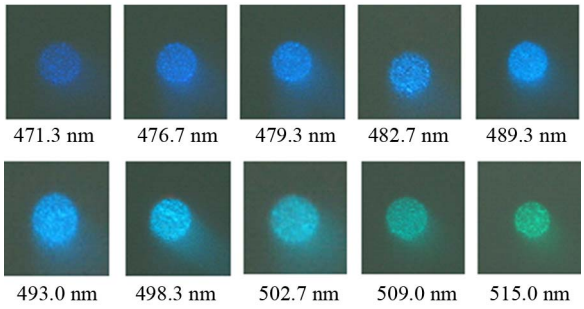

Fig. 7. (Color online) Blue–green light outputs by the self-cascaded SHG+SFG processes with wavelengths from 471.3 to 515 nm.

4. BANDWIDTH BROADENING DESIGN AND SIMULATION

To find out the potential tuning range of the cascaded χ^2 processes, a gradient-period QPM structure is considered as shown in Fig. 8(a). It was designed at a temperature of 25°C and a total length of ~6.4 mm. Slowly varying envelope approximation was used, and the propagation loss was ignored [21,22]. The coupled equations for the three wavelengths involved are

$$\frac{dA_\omega}{dz} + \frac{i}{2}\kappa A_{2\omega}^* A_{3\omega} e^{-i\Delta kz} = 0,$$

$$\frac{dA_{2\omega}^*}{dz} - \frac{i}{2}\kappa A_\omega A_{3\omega}^* e^{i\Delta kz} = 0,$$

$$\frac{dA_{3\omega}}{dz} + \frac{i}{2}\kappa A_\omega A_{2\omega} e^{i\Delta kz} = 0, \quad (2)$$

where $\Delta k \equiv k_{3\omega} - (k_{1\omega} + k_{2\omega})$ is the wave vector mismatch,

$$\kappa \equiv d\sqrt{\left(\frac{\mu}{\varepsilon_0}\right)\frac{(\omega)(2\omega)(3\omega)}{n_\omega n_{2\omega} n_{3\omega}}}$$

is the nonlinear coupling constant, $A_m \equiv (n_m/m)^{1/2}E_m$, $m = \omega, 2\omega, 3\omega$. E_ω is the input field, $E_{2\omega}$ is the SHG field, and $E_{3\omega}$ is the SFG field, which is generated from the E_ω and $E_{2\omega}$. When we used Eq. (2) to calculate SHG, $E_{2\omega}$ was replaced by E_ω and $E_{3\omega}$ was replaced by $E_{2\omega}$. A finite-difference time-domain method was adopted to simulate the nonlinear processes. In each incremental length, the SHG was simulated first, followed by SFG simulation to get the cascaded SHG+SFG. The incremental pitch of the structure is expressed as

$$d_i = d_0 + i\Delta d, \quad i = 0,1,2,\ldots,N\text{-}2,N\text{-}1, \quad (3)$$

where d_i is the segment length as shown in Fig. 8(a). Δd is the length increment. N is the pitch number. The total length was ~6.4 mm. Both d_0 and Δd were searched to optimize the gain-bandwidth product (GBP). It was found that if the pitch increment increases gradually, the broadened bandwidth becomes larger. The maximum total pitch increment was ~9 μm, and it is limited by the required pitch difference between the first-order SHG and the third-order SFG as shown in Fig. 1(a). The fluctuation of the bandwidth profile arises because the required domain-pitch difference between the first-order SHG and the third-order SFG is small. As illustrated in Fig. 8(b), the broadened bandwidth increases as the pitch increment increases for SHG, SFG, and self-cascaded SHG +SFG. It suggests that when the SHG and SFG bandwidth broadening are well designed, the self-cascaded

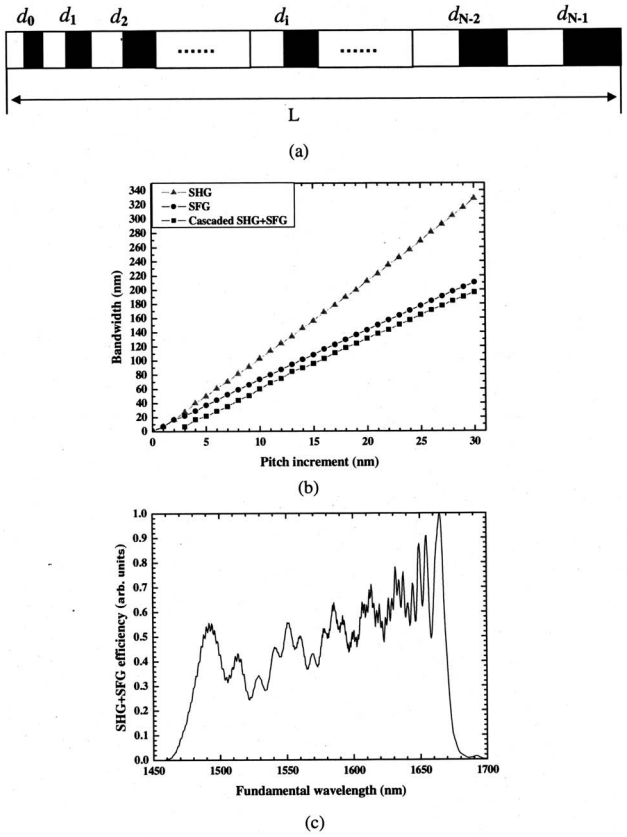

Fig. 8. (a) Gradient-period QPM structure for bandwidth broadening. (b) Broadened-bandwidth dependence on the pitch increments of SHG, SFG, and self-cascaded SHG+SFG. (c) Self-cascaded SHG+SFG conversion efficiency versus the fundamental wavelength for domain pitches from 16.79 to 25.79 μm.

SHG+SFG bandwidth can follow the trend. The simulated self-cascaded SHG+SFG conversion efficiency versus the fundamental wavelength for the gradient-pitch devices is shown in Fig. 8(c). When Δd equals 30 nm, the optimal 3 dB bandwidth was 196 nm for fundamental wavelength from 1476 to 1672 nm, and the required pitch ranges are 16.79 to 25.79 μm. This indicates the possibility of broadband tuning of the self-cascaded SHG+SFG mechanism. The gain that we used to calculate the GBP is defined as the wavelength-converted power divided by the input power. Both GBPs of SHG and SFG increase slightly, when the bandwidths are broadened as shown in Fig. 9. It implies that when the bandwidths are broadened by pitch increment, the increasing slopes of bandwidth are greater than the decreasing slopes of gain in both SHG and SFG cases. However, in the self-cascaded SHG+SFG case, it is the other way around. The GBP of the self-cascaded SHG+SFG decreases drastically when the bandwidths are broadened.

5. CONCLUSIONS

Good quality ZnO:PPLNCF samples were grown with feedback control of heating laser power to within 0.3% variation in fiber diameter. At a domain pitch of 15.45 μm, self-cascaded first-order SHG and third-order SFG was used to generate tunable blue–green light. The

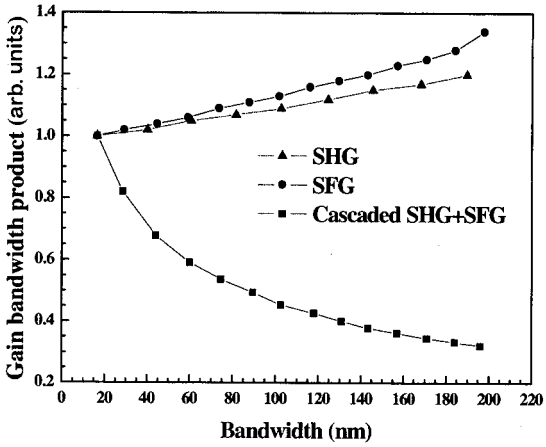

Fig. 9. Changes of GBPs for the SHG, SFG, and self-cascaded SHG+SFG, when bandwidths are getting wider.

measured SHG power at 714.2 nm was 12.25 mW under 100 mW input power and the self-cascaded SHG+SFG power measured at 477.1 nm was ~700 μW under 350 mW input power. The maximum internal efficiency of the SHG is 14.84% near 1431 nm. The tuning range of the self-cascaded SHG+SFG tunable blue–green light was more than 40 nm from 471.3 to 515 nm. Using a gradient-period structure, a 3 dB bandwidth of 196 nm for fundamental wavelength from 1476 to 1672 nm can be achieved by simulation. The GBP for the SHG or SFG processes slightly increases; while that of the self-cascaded SHG+SFG decreases drastically as the bandwidths are broadened.

ACKNOWLEDGMENTS

The authors thank Tao-Yuan Chang for helpful discussions. This work is partially supported by the National Science Council, Taiwan.

REFERENCES

1. L. F. Johnson and A. A. Ballman, "Coherent emission from rare earth ions in electro-optic crystals," J. Appl. Phys. **40**, 297–302 (1969).
2. T. Y. Fan, G. J. Dixon, and R. L. Byer, "Efficient GaAlAs diode-laser-pumped operation of Nd:YLF at 1.047 μm with intracavity doubling to 523.6 nm," Opt. Lett. **11**, 204–206 (1986).
3. M. M. Fejer, G. A. Magel, D. H. Jundt, and R. L. Byer, "Quasi-phase-matched second harmonic generation: tuning and tolerances," IEEE J. Quantum Electron. **28**, 2631–2654 (1992).
4. J. Zimmermann, J. Struckmeier, M. R. Hofmann, and J. P. Meyn, "Tunable blue laser based on intracavity frequency doubling with a fan-structured periodically poled $LiTaO_3$ crystal," Opt. Lett. **27**, 604–606 (2002).
5. S. E. Harris, "Tunable optical parametric oscillators," Proc. IEEE **58**, 2096–2113 (1969).
6. R. A. Baumgartner and R. L. Byer, "Optical parametric amplification," IEEE J. Quantum Electron. **QE-15**, 432–444 (1979).
7. L. Myers, R. Eckardt, M. M. Fejer, R. Byer, W. Bosenberg, and J. Pierce, "Quasi-phase-matched optical parametric oscillators in bulk periodically poled $LiNbO_3$," J. Opt. Soc. Am. B **12**, 2102–2116 (2002).
8. K. Kato, "Second-harmonic and sum-frequency generation

to 4950 and 4589 Å in KTP," IEEE J. Quantum Electron. **QE-24**, 3–4 (1988).
9. P. Xu, K. Li, G. Zhao, S. N. Zhu, Y. Du, S. H. Ji, Y. Y. Zhu, N. B. Ming, L. Luo, K. F. Li, and K. W. Cheah, "Quasi-phase-matched generation of tunable blue light in a quasi-periodic structure," Opt. Lett. **29**, 95–97 (2004).
10. C. K. Lee, J. Y. Zhang, J. Y. J. Huang, and C. L. Pan, "Theoretical and experimental studies of tunable ultraviolet-blue femtosecond pulses in a 405-nm pumped type I β-BaB_2O_4 noncollinear optical parametric amplifier and cascading sum-frequency generation," J. Opt. Soc. Am. B **21**, 1494–1499 (2004).
11. J. A. Armstrong, N. Bloembergen, J. Ducuing, and P. S. Pershan, "Interactions between light waves in a nonlinear dielectric," Phys. Rev. **127**, 1918–1939 (1962).
12. L. E. Myers, G. D. Miller, R. C. Eckardt, M. M. Fejer, and R. L. Byer, "Quasi-phase-matched 1.064-μm-pumped optical parametric oscillator in bulk periodically poled $LiNbO_3$," Opt. Lett. **20**, 52–54 (1995).
13. X.-M. Liu, H.-Y. Zhang, Y.-L. Guo, and Y.-H. Li, "Optimal design and applications for quasi-phase-matching three-wave mixing," IEEE J. Quantum Electron. **38**, 1225–1233 (2002).
14. M. Taya, M. C. Bashaw, and M. M. Fejer, "Photorefractive effects in periodically poled ferroelectrics," Opt. Lett. **21**, 857–859 (1996).
15. D. H. Jundt, "Lithium niobate single crystal fiber growth and quasi-phase matching," Ph.D. dissertation (Stanford University, 1991).
16. L. M. Lee, C. C. Kuo, J. C. Chen, T. S. Chou, Y. C. Cho, S. L. Huang, and H. W. Lee, "Periodical poling of MgO doped lithium niobate crystal fiber by modulated pyroelectric field," Opt. Commun. **253**, 375–381 (2005).
17. L. Becouarn, E. Lallier, M. Brevignon, and J. Lehoux, "Cascaded second-harmonic and sum-frequency generation of a CO_2 laser by use of a single quasi-phase-matched GaAs crystal," Opt. Lett. **23**, 1508–1510 (1998).
18. Y. Zhang, Y. H. Xu, M. H. Li, and Y. Q. Zhao, "Growth and properties of Zn doped lithium niobate crystal," J. Cryst. Growth **233**, 537–540 (2001).
19. D. H. Jundt, "Temperature-dependent Sellmeier equation for index of refraction, n_e, in congruent lithium niobate," Opt. Lett. **22**, 1553–1555 (1997).
20. C. S. Yu and A. H. Kung, "Grazing-incidence periodically poled $LiNbO_3$ optical parametric oscillator," J. Opt. Soc. Am. B **16**, 2233–2238 (1999).
21. A. Yariv, *Optical Electronics in Modern Communications*, 5th ed. (Oxford U. Press, 1997), pp. 285–293.
22. P. S. Banks, M. D. Feit, and M. D. Perry, "High-intensity third-harmonic generation," J. Opt. Soc. Am. B **19**, 102–118 (2002).